Chinese Chemical Letters 33 (2022) 1381–1384

Contents lists available at ScienceDirect

Chinese Chemical Letters

journal homepage: www.elsevier.com/locate/cclet

Four-step spin-crossover in an oxamide-decorated metal-organic framework

Siguo Wu[1], Sukhen Bala[1], Zeyu Ruan, Guozhang Huang, Zhaoping Ni*, Mingliang Tong

Key Laboratory of Bioinorganic and Synthetic Chemistry of Ministry of Education, School of Chemistry, Sun Yat-Sen University, Guangzhou 510275, China

ARTICLE INFO

Article history:
Received 31 May 2021
Revised 18 June 2021
Accepted 5 August 2021
Available online 11 August 2021

Keywords:
Spin crossover
Oxamide
Metal-organic framework
Hofmann-type
Host-guest interaction

ABSTRACT

Spin-crossover (SCO) complexes with multiple spin states are promising candidates for high-order magnetic storage and multiple switches. Here, by employing the *N,N′*-4-dipyridyloxalamide (dpo) ligand, we synthesize two Hofmann-type metal-organic frameworks (MOFs) $[Fe(dpo)\{Ag(CN)_2\}_2]\cdot 3DMF$ (**1**) and $[Fe(dpo)\{Ag(CN)_2\}_2]\cdot 0.5MeCN\cdot 2DEF$ (**2**), which exhibit guest dependent four-step SCO behaviors with the sequences of LS → $\sim LS_{2/3}HS_{1/3}$ → $LS_{1/2}HS_{1/2}$ → $\sim LS_{3/10}HS_{7/10}$ → HS and LS → $\sim LS_{2/3}HS_{1/3}$ → $LS_{1/2}HS_{1/2}$ → $\sim LS_{1/4}HS_{3/4}$ → HS, respectively. Therefore, the incorporation of hydrogen-donating/hydrogen-accepting groups into the Hofmann-type MOFs may effectively explore the multi-step SCO materials by tuning hydrogen-bonding interactions.

Multi-stable materials have aroused significant interests in scientific community for their potential applications in informatics. Spin-crossover (SCO) complexes, especially for iron(II) species whose spin states can be manipulated between diamagnetic low-spin (LS, $t_{2g}^6e_g^0$) state and paramagnetic high-spin (HS, $t_{2g}^4e_g^2$) state via external stimuli (such as temperature, pressure, light irradiation and guest molecules), are conceivable elements for memory devices and opto-magnetic switches [1-5]. When the competitions of long-range ferro- and antiferro-elastic interactions occur between SCO units, elastic frustrations may lead to multi-step SCO behaviors, which can act as the multi-stable materials with the potential applications in high-order data storage and multi-switches [6-8].

Hofmann-type clathrates, consist of iron-cyanometalate meshes and pillar ligands, are promising candidates for constructing high-performance SCO materials [9-11]. Extensive efforts have been devoted to promote the SCO cooperativity *via* fine-tuning the hydrogen-bonding interactions [12-14] and π-π interactions [15,16]. By means of guest exchange, the implementations of guest programmable multistep switches, gate-opening with multiplex responses and bidirectional chemo-switching have been achieved in porous 2D/3D Hofmann-type frameworks [17-20]. However, the synergetic effects of host-guest interactions are complicated since SCO dynamics are influenced by the size, distribution and geometry of the guests, the porous capacity and characteristic of the host as well as the direction and strength of host-guest interactions [11]. Integration of hydrogen-donating/hydrogen-accepting groups (imide [21], amide [22], amino [18], hydroxyl [14,23], urea [24], *etc.*) into pillar ligands would be a judicious choice for achieving strong host-guest interactions in Hofmann-type metal-organic frameworks (MOFs).

Since hydrogen-bonding interactions play an important role in multi-step SCO behaviors [12-14,18], an oxamide-decorated ligand *N,N′*-4-dipyridyloxalamide (dpo, Scheme 1) is firstly employed to construct two SCO Hofmann-type MOFs $[Fe(dpo)\{Ag(CN)_2\}_2]\cdot 3DMF$ (**1**) and $[Fe(dpo)\{Ag(CN)_2\}_2]\cdot 0.5MeCN\cdot 2DEF$ (**2**), in which the oxamide unit can act as hydrogen bond donor as well as acceptor. Hence, four-step SCO behaviors with two new sequences are observed, although the reported four-step spin transition properties are extremely rare so far [12,14,16,18,22,25-27]. Moreover, spin transition temperatures and thermal hysteresis loops are altered by different solvent guests.

Complexes **1** and **2** were prepared by slow diffusion methods and isolated as the yellow block crystals. The crystalline samples were assessed by elemental analysis, powder X-ray diffraction (Figs. S1 and S2 in Supporting information), thermogravimetric (TG) measurements (Figs. S3 and S4 in Supporting information) and infrared spectra (Figs. S5 and S6 in Supporting information). TG analyses reveal that the guest molecules in **1** and **2** can be completely removed upon heating to around 435 and 473 K, respectively.

Temperature-dependent magnetic susceptibility measurements for **1** and **2** were performed over the range of 10−300 K with a sweep rate of 2 K/min (Fig. 1). At room temperature, the $\chi_M T$

* Corresponding author.
E-mail address: nizhp@mail.sysu.edu.cn (Z. Ni).
[1] These authors contributed equally to this work.

https://doi.org/10.1016/j.cclet.2021.08.012
1001-8417/

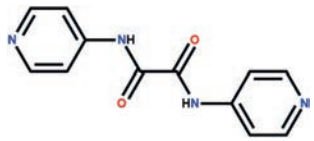

Scheme 1. Representation of the dpo ligand.

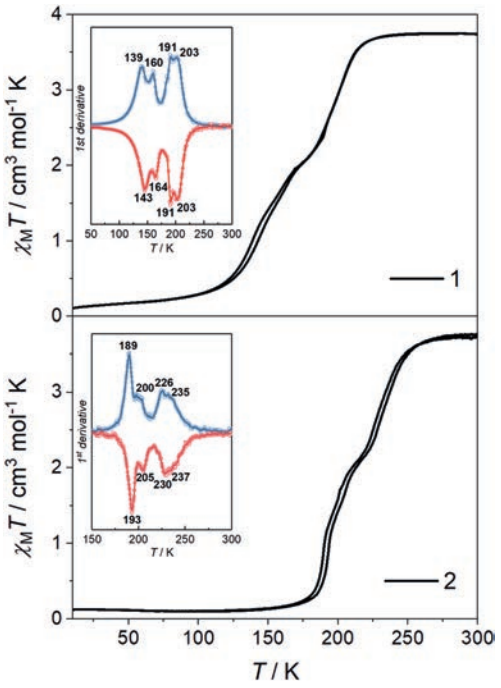

Fig. 1. Variable-temperature magnetic susceptibility for **1** and **2** with a sweep rate of 2 K/min. Inset: 1st derivative plots of $\chi_M T$ curves. The blue and red lines represent for the cooling and warming modes, respectively.

value of **1** is close to 3.75 cm^3 K/mol, indicating a pure HS state. It slightly decreases to 3.65 cm^3 K/mol at 230 K and then declines gradually. An inclined plateau is observed in the middle of SCO curve, corresponding to a $HS_{1/2}LS_{1/2}$ intermediate state. Upon further cooling, the $\chi_M T$ value reaches to 0.11 cm^3 K/mol at 10 K, which is consistent with a LS state. The 1st derivative plot of magnetic data suggests four-step SCO behavior with a sequence of LS→~$LS_{2/3}HS_{1/3}$→$LS_{1/2}HS_{1/2}$→~$LS_{3/10}HS_{7/10}$→HS, although their magnetic plateaus are not obvious. The critical temperatures for the peaks/valleys are at 139/160/191/203 K and 143/164/191/203 K in the cooling/warming modes, respectively. Therefore, the largest width of thermal hysteresis (ΔT) loop is only ~4 K.

For **2**, the cooling and warming SCO curves with hysteresis loop shift to the higher temperature region. A gradual four-step SCO behavior with the sequence of LS → ~$LS_{2/3}HS_{1/3}$ → $LS_{1/2}HS_{1/2}$ → ~$LS_{1/4}HS_{3/4}$ → HS can be inferred from the differential magnetic curve, although no obvious magnetic plateaus are observed in **2**. The related 1st derivative peaks/valleys locate at 189/200/226/235 K and 193/205/230/237 K in the cooling/warming modes, indicating the thermal hysteresis width is up to 5 K. The four-step SCO behaviors of **1** and **2** are further confirmed by two cycles of magnetization measurements (Figs. S7 and S8 in Supporting information).

To corroborate the multi-step SCO behaviors, DSC measurements were carried out with a sweeping rate of 10 K/min. As shown in Fig. S9 (Supporting information), four pairs of exothermic/endothermic peaks locate at 136/149/186/195 K and 144/158/189/199 K in the cooling/warming modes, respectively, which confirms the four-step SCO behavior in **1**. These DSC peaks slightly deviate from the T_c peaks from the magnetic data, which should be due to the different scanning rates. Analogously, four sets of exothermic (193/201/226/235 K) and endothermic (195/204/228/238 K) peaks are found in the cooling and warming modes, confirming the four-step SCO behavior in **2** (Fig. S10 in Supporting information). The total enthalpy changes (ΔH) of **1** and **2** are around 13.21 and 9.84 kJ/mol, which are in the normal range for SCO Fe^{II} compounds [28].

Complex **1** crystalizes in triclinic space group and retains the geometric symmetry at 120, 182 and 298 K (Table S1 in Supporting information). The asymmetry unit consists of a Fe^{II} ion, a dpo pillar ligand, two $[Ag(CN)_2]^-$ linkers and three DMF molecules (Fig. 2a). Each Fe^{II} center adopts a distorted octahedral geometric fashion with $[FeN_6]$ coordination environment. The equatorial positions are occupied by CN groups of linear $[Ag(CN)_2]^-$ ligands, giving rise to the $[Fe\{Ag(CN)_2\}_2]_\infty$ network. The Fe^{II} ions between the adjacent layers are axially linked by the bidentate dpo ligands, which results a two-fold interpenetration framework (Fig. 2c). Permanent 1D channels along the diagonal direction of the *a* and *b* axis are found, wherein three DMF guests are housed (Fig. S11 in Supporting information). Two DMF molecules are involved into the strong N−H···O hydrogen bonds on either side of the dpo ligand (green dotted lines in Fig. 2a). Meanwhile, the remaining DMF molecule is engaged in the weak intermolecular interactions with the neighboring DMF guest (purple dotted line in Fig. 2b) and dpo ligand.

The detailed structural parameters of **1** can give a clue of the stepped SCO behavior, although only one unique Fe^{II} ion is solved in the intermediate state (Table S3 in Supporting information). At 120 and 298 K, the average Fe−N bond length is 1.963 and 2.178 Å, in line with the LS and HS Fe^{II} ions, respectively. In contrast, the $<Fe-N>_{av}$ distance is 2.099 Å at 182 K, which is close to the $LS_{1/2}HS_{1/2}$ state. Meanwhile, the octahedral distortion parameter (Σ) changes from 11.67° (120 K) to 11.49° (182 K) and then to 16.00° (298 K). Since the HS Fe^{II} ions favor higher Σ values than their LS counterparts, the unusual Σ at 182 K hints the presence of antiferro-elastic interaction, which is required for the stepped SCO system to stabilize the intermediate states according to the elastic model [6]. Upon warming, the monotonic increases of the unit cell volume and the Fe···Fe distances along the dpo and $[Ag(CN)_2]^-$ linkers as well as the Ag···Ag distance are consistent with the SCO process, which represent the ferro-elastic interactions. The N3···O3 distance and N3−H3···O3 angle are monotonically increased and decreased. Meanwhile, the unusual trend of the N2···O4 distance change and the monotonic increase of N2−H2···O4 angle are found. Hence, the complicated hydrogen-bonding interactions between host and guest hint the competition between antiferro- and ferro-elastic interactions [29].

Complex **2** possesses a similar two-fold interpenetration framework with 1D channel along the *b* axis (Fig. S12 in Supporting information) but crystalizes in orthorhombic space group $Pca2_1$ at 120, 215 and 300 K. Unlike **1**, the asymmetric unit in **2** contains two crystallographically inequivalent Fe^{II} ions, two dpo ligands as well as four $[Ag(CN)_2]^-$ linkers belonging to two sets of 3D frameworks. Meanwhile, one MeCN and four DEF serve as the guest molecules (Fig. 3). Most importantly, one DEF form a bifurcated H-bond (N3−H3···O7···H10−N10) with two dpo ligands from two 3D frameworks, which may contribute to the asymmetry of two-fold interpenetration framework and improve their effective transmission via host-guest interactions. The remaining amide groups in two dpo ligands separately generate the strong hydrogen-bonding interactions (N2−H2···O5 and N11−H11···O8) with two DEF molecules. The remaining DEF and MeCN molecules are only involved into the van der Waals interactions with the neighboring DEF guests.

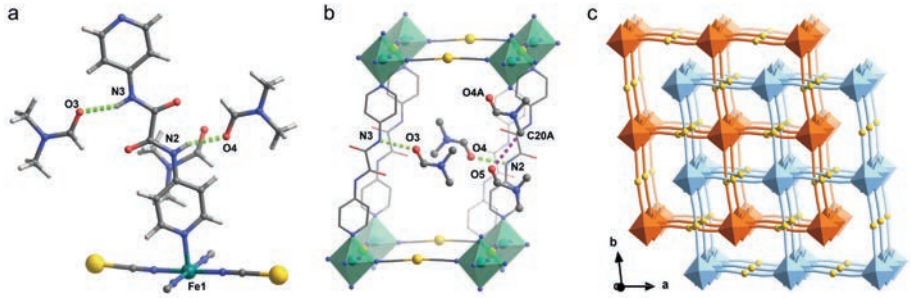

Fig. 2. (a) The asymmetric unit, (b) hydrogen-bonding interactions and (c) two-fold interpenetration framework in **1**. Color code: Fe^{II}, green; Ag, golden; O, red; N, blue; C, grey, H, off-white. Green/purple dotted lines represent for the strong host-guest H-bonds/the weak guest-guest H-bonds.

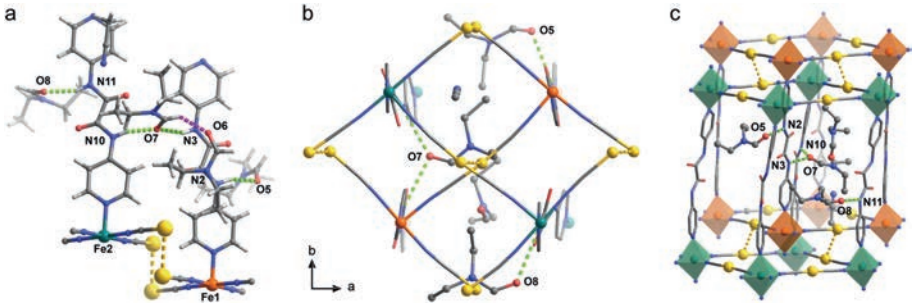

Fig. 3. (a) The asymmetric unit, (b) hydrogen-bonding interactions viewed along *c* axis and (c) two-fold interpenetration framework in **2**. Color code: Fe^{II}, orange/green; Ag, golden; O, red; N, blue; C, grey, H, off-white. Green/purple/golden dotted lines represent for host-guest H-bonds/guest-guest H-bonds/argentophilic interactions.

After carefully checking the single-crystal diffraction patterns, no superstructures [30] are found in **2** amid spin transition. The structural parameters of two inequivalent Fe^{II} sites in **2** are further explored in detail. The $<Fe1-N>_{av}/<Fe2-N>_{av}$ distances are 1.960/1.968, 2.056/2.077 and 2.171/2.184 Å at 120, 215 and 300 K, matching well with the LS, $LS_{1/2}HS_{1/2}$ and HS states, respectively, (Table S4 in Supporting information). Despite the similar variation of the $<Fe-N>_{av}$ distance, the octahedral distortion parameters Σ show different tendency for Fe1 and Fe2 ions. ΣFe2 increases monotonically in the order of 14.38° → 15.9° → 19.1° upon warming. However, ΣFe1 decreases from 13.92° at 120 K to 13.3° at 215 K and then increases to 14.8° at 300 K, indicating the contribution of antiferro-elastic interaction in the $LS_{1/2}HS_{1/2}$ state. The unit cell volume, the Fe···Fe distances within the 3D framework and the Ag···Ag distances between two 3D frameworks increase monotonically upon warming, which contribute to the ferro-elastic interactions. The N···O distances and N–H···O angles in the bifurcated H-bond are monotonically increased and decreased, respectively, suggesting the ferro-elastic interactions between this guest and two 3D frameworks. Meanwhile, the other two strong hydrogen-bonding interactions are complicated, in which the N···O distances increase while the N–H···O angles show abnormal changes.

By introducing different guest molecules, complexes **1** and **2** exhibit four-step SCO behaviors with different spin transition temperatures and thermal hysteresis loops. To explore the magnetostructural relationship between **1** and **2**, the structural data in the HS state are compared in detail. **1** and **2** possess the same structural components and topological network for the twofold-interpenetrated frameworks and the similar $<Fe-N>_{av}$ distance at the room temperature. However, the total guest volume in **2** is larger than that in **1**, which should empirically result in the lower T_c value if only considering the effect of guest size [11]. Meanwhile, in order to adapt to the different sizes of solvent guests and host-guest interactions, the structural parameters of the framework are regulated accordingly. The average Fe–N≡C angles of 172.10° and 171.68° for Fe1 and Fe2 ions in **2** are larger than that in **1** (170.57°), which should result in the higher T_c value [14]. Therefore, the competition of the effects of larger guest size and Fe–N≡C angle gives rise to the higher T_c value in **2**. In addition, the shorter Ag···Ag distance between two 3D frameworks in **2** contributes positively to the SCO cooperativity. When comparing the strong hydrogen-bonding interactions, the longer N···O distances and the smaller N–H···O angles are found in **2**, which give negative contributions to SCO cooperativity. However, the bifurcated H-bond in **2** can directly link two sets of 3D frameworks and build new path to transmit the SCO cooperativity. Therefore, the improved hysteresis loop in **2** may result from the contributions of the stronger argentophilic interactions and the bifurcated H-bond.

In summary, we successfully constructed two Hofmann-type SCO complexes $[Fe(dpo)\{Ag(CN)_2\}_2]\cdot 3DMF$ (**1**) and $[Fe(dpo)\{Ag(CN)_2\}_2]\cdot 0.5MeCN\cdot 2DEF$ (**2**) by utilizing oxamide-functionalized ligand, which provided a platform to tune SCO behavior *via* hydrogen-bonding interactions. Accordingly, the framework adapted to the different guests and then exhibited different SCO behaviors. The magnetic data displayed four-step SCO behaviors with the sequence of $LS \rightarrow {\sim}LS_{2/3}HS_{1/3} \rightarrow LS_{1/2}HS_{1/2} \rightarrow {\sim}LS_{3/10}HS_{7/10} \rightarrow HS$ and $LS \rightarrow {\sim}LS_{2/3}HS_{1/3} \rightarrow LS_{1/2}HS_{1/2} \rightarrow {\sim}LS_{1/4}HS_{3/4} \rightarrow HS$ for **1** and **2** respectively. The higher T_c in **2** resulted from the competitive contributions of guest size effect and the larger Fe–N≡C angle. Meanwhile, the improved SCO cooperativity in **2** resulted from the contributions of the argentophilic interactions and bifurcated H-bond. In the future, this oxamide-decorated ligand can extend to other Hofmann-type system by altering the cyanometallate, which may yield fruitful SCO behaviors *via* hydrogen-bonding interactions.

Declaration of competing interest

The authors declared that they have no conflicts of interest to this work. We declare that we do not have any commercial or associative interest that represents a conflict of interest in connection with the work submitted.

Acknowledgment

This work was supported by the National Key Research and Development Program of China (No. 2018YFA0306001), the National Natural Science Foundation of China (Nos. 21950410521, 21771200 and 21773316), and the Pearl River Talent Plan of Guangdong (No. 2017BT01C161).

Supplementary materials

Supplementary material associated with this article can be found, in the online version, at doi:10.1016/j.cclet.2021.08.012.

References

[1] P. Gütlich, H.A. Goodwin, Spin crossover in transition metal compounds I-III. In Top. Curr. Chem., Springer-Verlag: Berlin, 2004, pp. 233-235.
[2] M.A. Halcrow, Spin-Crossover Materials: Properties and Applications, John Wiley and Sons Ltd., West Sussex, 2013.
[3] S.I. Ohkoshi, K. Imoto, Y. Tsunobuchi, et al., Nat. Chem. 3 (2011) 564–569.
[4] H. Zheng, Y.S. Meng, G.L. Zhou, et al., Angew. Chem. Int. Ed. 57 (2018) 8468–8472.
[5] R.W. Hogue, S. Singh, S. Brooker, Chem. Soc. Rev. 47 (2018) 7303–7338.
[6] M. Paez-Espejo, M. Sy, K. Boukheddaden, J. Am. Chem. Soc. 138 (2016) 3202–3210.
[7] J. Cruddas, B.J. Powell, J. Am. Chem. Soc. 141 (2019) 19790–19799.
[8] L. Piñeiro-López, F.J. Valverde-Muñoz, E. Trzop, et al., Chem. Sci. 12 (2021) 1317–1326.
[9] T. Kitazawa, Y. Gomi, M. Takahashi, et al., J. Mater. Chem. 6 (1996) 119–121.
[10] P.D. Southon, L. Liu, E.A. Fellows, et al., J. Am. Chem. Soc. 131 (2009) 10998–11009.
[11] Z.P. Ni, J.L. Liu, M.N. Hoque, et al., Coord. Chem. Rev. 335 (2017) 28–43.
[12] J.E. Clements, J.R. Price, S.M. Neville, et al., Angew. Chem. Int. Ed. 55 (2016) 15105–15109.
[13] C.H. Pham, J. Cirera, F. Paesani, J. Am. Chem. Soc. 138 (2016) 6123–6126.
[14] N.F. Sciortino, K.A. Zenere, M.E. Corrigan, et al., Chem. Sci. 8 (2017) 701–707.
[15] T. Delgado, M. Meneses-Sánchez, L. Piñeiro-López, et al., Chem. Sci. 9 (2018) 8446–8452.
[16] C.J. Zhang, K.T. Lian, G.Z. Huang, et al., Chem. Commun. 55 (2019) 11033–11036.
[17] M.J. Murphy, K.A. Zenere, F. Ragon, et al., J. Am. Chem. Soc. 139 (2017) 1330–1335.
[18] W. Liu, Y.Y. Peng, S.G. Wu, et al., Angew. Chem. Int. Ed. 56 (2017) 14982–14986.
[19] R. Turo-Cortés, C. Bartual-Murgui, J. Castells-Gil, et al., Chem. Sci. 11 (2020) 11224–11234.
[20] M. Ohba, K. Yoneda, G. Agusti, et al., Angew. Chem. Int. Ed. 48 (2009) 4767–4771.
[21] Y. Meng, Y.J. Dong, Z. Yan, et al., Cryst. Growth Des. 18 (2018) 5214–5219.
[22] F.J. Valverde-Muñoz, C. Bartual-Murgui, L. Piñeiro-López, et al., Inorg. Chem. 58 (2019) 10038–10046.
[23] A.T. Brennan, K.A. Zenere, C.J. Kepert, et al., Inorg. Chem. 60 (2021) 3871–3878.
[24] D.J. Mondal, S. Roy, J. Yadav, et al., Inorg. Chem. 59 (2020) 13024–13028.
[25] C.J. Zhang, K.T. Lian, S.G. Wu, et al., Inorg. Chem. Front. 7 (2020) 911–917.
[26] M. Nihei, H. Tahira, N. Takahashi, et al., J. Am. Chem. Soc. 132 (2010) 3553–3560.
[27] A. Sugaya, S. Ueno, J. Okabayashi, et al., New J. Chem. 38 (2014) 1955–1958.
[28] P. Gütlich, A. Hauser, H. Spiering, Angew. Chem. Int. Ed. 33 (1994) 2024–2054.
[29] M. Feng, Z.Y. Ruan, Y.C. Chen, et al., Chem. Commun. 56 (2020) 13702–13718.
[30] N.F. Sciortino, K.R. Scherl-Gruenwald, G. Chastanet, et al., Angew. Chem. Int. Ed. 51 (2012) 10154–10158.